Template for Preparation of Manuscripts for *Nano Research*

This template is to be used for preparing manuscripts for submission to *Nano Research*. Use of this template will save time in the review and production processes and will expedite publication. However, use of the template is not a requirement of submission. Do not modify the template in any way (delete spaces, modify font size/line height, etc.). If you need more detailed information about the preparation and submission of a manuscript to Nano Research, please see the latest version of the Instructions for Authors at http://www.thenanoresearch.com/.

TABLE OF CONTENTS (TOC)

Authors are required to submit a graphic entry for the Table of Contents (TOC) in conjunction with the manuscript title. This graphic should capture the readers' attention and give readers a visual impression of the essence of the paper. Labels, formulae, or numbers within the graphic must be legible at publication size. Tables or spectra are not acceptable. Color graphics are highly encouraged. The resolution of the figure should be at least 600 dpi. The size should be at least 50 mm × 80 mm with a rectangular shape (ideally, the ratio of height to width should be less than 1 and larger than 5/8). One to two sentences should be written below the figure to summarize the paper. To create the TOC, please insert your image in the template box below. Fonts, size, and spaces should not be changed.

Water-Assisted Self-Sustained Burning of Metallic Single-Walled Carbon Nanotubes toward Scalable Transistor Fabrication

Keigo Otsuka[1], Taiki Inoue[1], Yuki Shimomura[1], Shohei Chiashi[1], and Shigeo Maruyama[1,2]*

[1] The University of Tokyo, Japan

[2] National Institute of Advanced Industrial Science and Technology (AIST), Japan

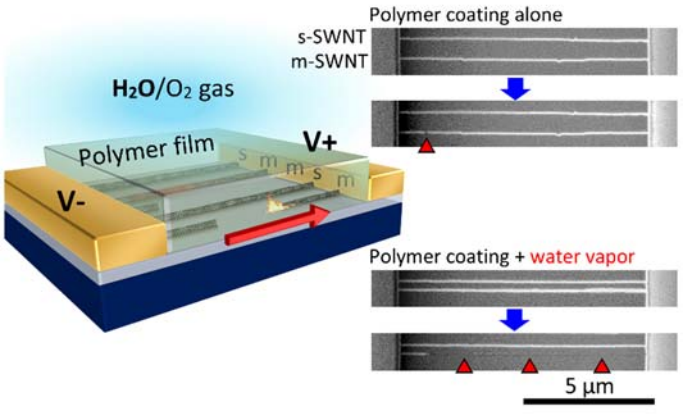

The burning of on-substrate carbon nanotubes is self-propagated with the assistance of water vapor exposure and polymer-coating. Semiconducting carbon nanotube arrays are obtained by selectively burning metallic tubes.

Shigeo Maruyama, http://www.photon.t.u-tokyo.ac.jp

Nano Research
DOI (automatically inserted by the publisher)
Research Article
ISSN 1998-0124
CN 11-5974/O4

Water-Assisted Self-Sustained Burning of Metallic Single-Walled Carbon Nanotubes toward Scalable Transistor Fabrication

Keigo Otsuka[1], Taiki Inoue[1], Yuki Shimomura[1], Shohei Chiashi[1], and Shigeo Maruyama[1,2]

[1] *Department of Mechanical Engineering, The University of Tokyo, 7-3-1 Hongo, Bunkyo-ku, Tokyo 113-8656, Japan*
[2] *Energy NanoEngineering Lab., National Institute of Advanced Industrial Science and Technology (AIST), 1-2-1 Namiki, Tsukuba, 305-8564, Japan*

Received: day month year
Revised: day month year
Accepted: day month year (automatically inserted by the publisher)

KEYWORDS
single-walled carbon nanotube, field-effect transistor, selective removal, electrical breakdown, one-way burning

ABSTRACT

Although aligned arrays of semiconducting single-walled carbon nanotubes (s-SWNTs) are promising for use in next-generation electronics due to their ultrathin bodies and ideal electrical properties, even a small portion of metallic (m-) counterparts causes excessive leakage in field-effect transistors (FETs). To fully exploit the benefits of s-SWNTs for the use in large-scale systems, it is necessary to completely eliminate m-SWNTs from as-grown SWNT arrays and thereby to obtain purely semiconducting arrays in a large area, where a number of FETs can be built with a flexibility in the design. Here, we present the electrical burning of m-SWNTs assisted by water vapor and polymer-coating to achieve the elimination of m-SWNTs in long length toward the scalable fabrication of transistors from the remaining s-SWNT arrays. During the electrical breakdown process, the combination of water vapor and polymer-coating significantly enhances the burning of SWNTs, which results in self-sustained reaction along the nanotube axis. We found that m-SWNT segments partially remaining on the anode side resulted from one-way burning from initial breakdown position where Joule-heating-induced oxidation first occurs. The s-SWNT-enriched arrays obtained were used to fabricate multiple FETs with a high on-off current ratio. The results demonstrate the advantages of this approach over conventional electrical breakdown for the large-scale purification of s-SWNTs.

1 Introduction

Densely-packed arrays of semiconducting single-walled carbon nanotubes (s-SWNTs) are a promising material for high-performance field-effect transistor (FET) channels [1,2]. Lattice-oriented SWNT growth has been used to realize highly aligned individual SWNTs on single-crystal substrates [3,4]. In addition to the orientation, control of the SWNT density is also very important; therefore, much effort has been invested to improve the density through catalyst

Address correspondence to Shigeo Maruyama, email; maruyamma@photon.t.u-tokyo.ac.jp

design and by multiple-cycle growth or transfer [5–9]. The as-grown SWNT array always contains metallic (m-) SWNTs, which significantly degrade the device performance. Liquid-based separation after synthesis has provided s-SWNTs of >99% purity, and dense and aligned arrays can be assembled after the separation process [10–13]. Selective growth of s-SWNTs directly on substrates has also been used to realize high-purity s-SWNTs and even single-chirality SWNTs [14–16], although these SWNTs still have to be further purified to reach the required purity (m-SWNTs <0.0001% [2]).

Post-growth removal of m-SWNTs from clean and highly aligned arrays directly grown on substrates is an especially powerful approach toward the realization of high-performance FETs [17–19]. Electrical breakdown induced by Joule self-heating selectively cuts m-SWNTs without damage to the s-SWNTs because the difference in the electric transport properties of the two types of SWNTs is directly utilized [17,20]. In addition, compatibility with high-density arrays (>100 SWNTs μm^{-1}) makes this method a suitable tool for the fabrication of high-performance FETs [21,22]. One of the drawbacks of electrical breakdown is the difficulty in large-scale fabrication of FETs because only local portions (ca. 100 nm) of m-SWNTs are removed and one-by-one voltage application is required for a number of electrode pairs. With regard to this drawback, electrical breakdown using comb-shaped temporal electrodes has been successfully demonstrated for chip-scale circuit fabrication [1,23]. However, electrical breakdown of ultrascaled devices faces degradation of the on-current retention because an extremely strong field is required to cut the m-SWNTs due to strong heat-sinking to the metal contacts [24,25].

We have recently proposed an extended method of electrical breakdown for the full-length removal of m-SWNTs, in which organic films are used to assist the propagation of SWNT burning [26]. This technique preserves the original advantages of electrical breakdown, including the high selectivity of removal between s- and m-SWNTs, and the applicability to high-density SWNT arrays. Moreover, a single treatment of full-length m-SWNT removal enables the robust integration of a number of FETs, even with short-channel lengths, and without sacrifice of the on current through the use of the resultant long s-SWNT arrays. However, variation in the burning length and limited reproducibility of the technique, which originate from a poor understanding of the mechanism for SWNT burning, must be resolved to establish this as a practical method.

Here, we present water- and polymer-assisted burning as an on-substrate purification method for the stable removal of long m-SWNTs. Poly(methyl methacrylate) (PMMA) is employed as an organic film material due to its ease of handling and well-characterized properties, though similar results were obtained with other polymer, such as polystyrene. The burning length of m-SWNTs is increased by an average of more than thirty times (>5 μm) by the introduction of water vapor into the ambient gas. Partial removal of m-SWNTs is attributed to one-way burning from a random position of breakdown. Multiple devices are then fabricated using the purified SWNT arrays to demonstrate the effectiveness of the water-assisted burning technique for large-scale purification. A simulation of SWNT burning is also conducted to elucidate the role of polymer films and to obtain further guidance toward successful full-length burning of m-SWNTs.

Note that throughout the study, the term burning represents the chain-reaction oxidation of the material, which propagates along SWNTs, while the term breakdown refers to the physical cutting of SWNTs induced by Joule self-heating. Therefore, the length of removal can only be defined for the burning phenomenon. The burning of SWNTs is electrically triggered but can be sustained without further electrical power input.

2 Results and discussion

2.1 Water- and polymer-assisted burning of m-SWNTs

The dependence of SWNT burning on the ambient gas conditions was investigated. The Joule heating-induced burning was initiated by application of a ramp voltage along the tube axis (see Methods). Two gas conditions were used for the burning of SWNTs

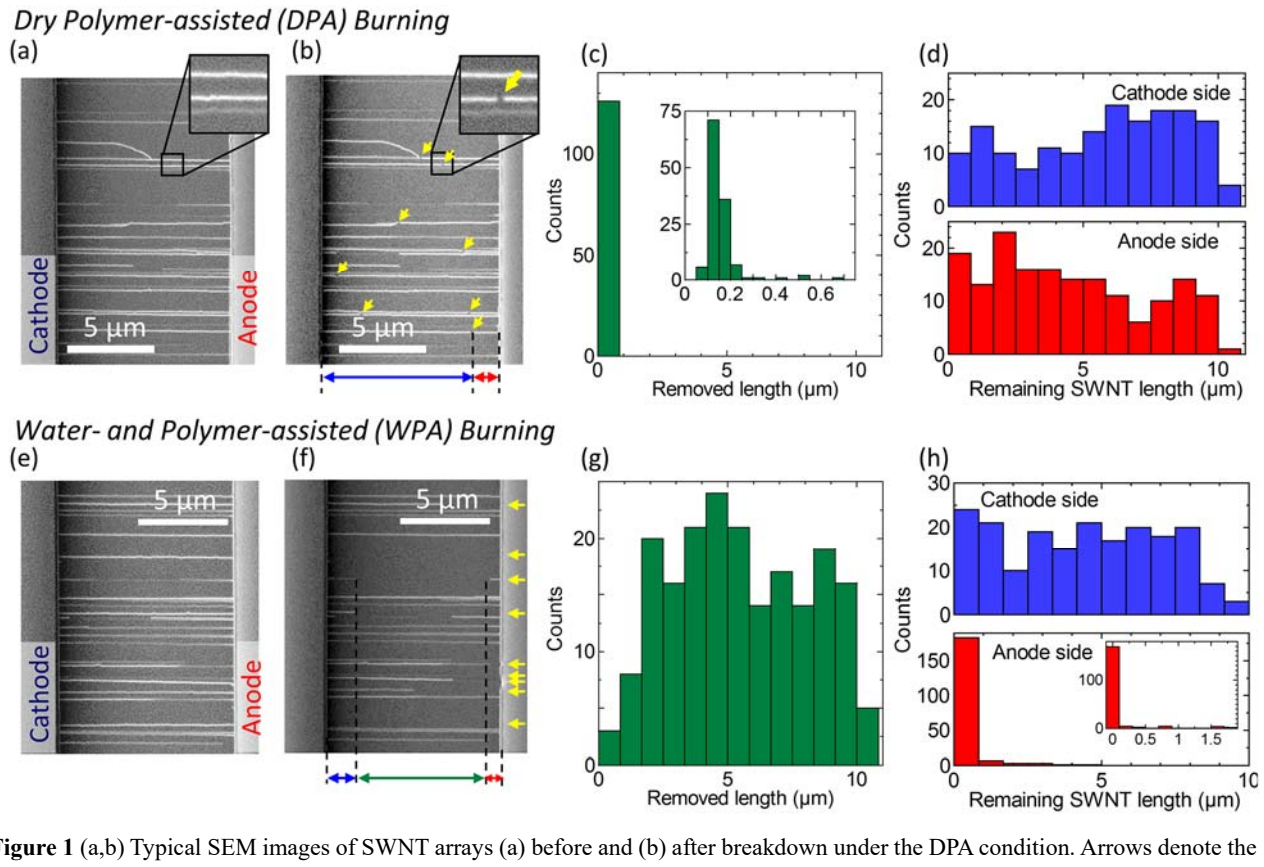

Figure 1 (a,b) Typical SEM images of SWNT arrays (a) before and (b) after breakdown under the DPA condition. Arrows denote the breakdown position. Distributions of (c) the removed length, and (d) the length of SWNTs remaining at both the cathode and anode sides. (e-h) Similar data for the SWNTs after WPA burning. (e,f) Typical SEM images of SWNT arrays (e) before and (f) after burning. Arrows denote the burned SWNTs. Distributions of (g) the removed length of SWNTs treated under the WPA condition, and (h) the remaining SWNT length.

embedded in PMMA thin films: (1) dry oxygen gas, and (2) oxygen gas saturated with water vapor at room temperature (wet oxygen). The former and latter are referred to as dry polymer-assisted (DPA), and water- and polymer-assisted (WPA) conditions, respectively. For both conditions, the total pressure was ca. 90 kPa.

Typical scanning electron microscopy (SEM) images before and after voltage application treatment (up to 60 V) of an array of 10-μm-long SWNTs under the DPA condition are shown in Fig. 1(a) and (b), respectively. The length of the removed portion was very small (ca. 160 nm on average), even with the PMMA film coating, as shown in Fig. 1(c). This indicates that the self-sustained burning of SWNTs cannot be achieved just with PMMA and pure oxygen. Note that the breakdown position was widely distributed in the channel in these experiments, while a previous study on in-air breakdown of shorter-channel FETs showed that the majority of SWNTs broke near the middle due to thermal dissipation to the metal electrodes [27]. The breakdown position in the present study might also be influenced by randomly occurring defects or buckling of SWNTs [28] which were derived from the growth and transfer process.

Figures 1(e-g) show typical SEM images before and after voltage application treatment of an array of 10-μm-long SWNTs under the WPA condition, and also the distribution of the removed length (burning length). The average removed length was significantly increased to 5.5 μm by the introduction of saturated water vapor into the system, which accounts for 53.7% of the total original length (10.3 μm). This result

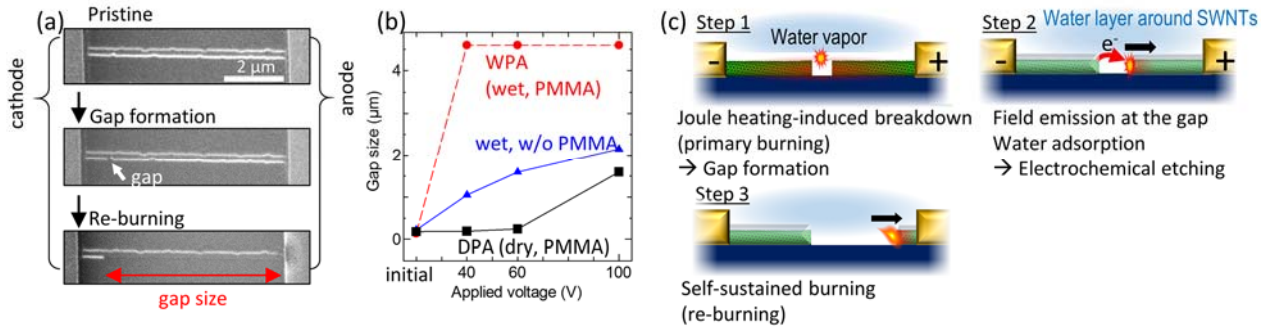

Figure 2 (a) SEM images of two parallel SWNTs at various stages. One of the SWNTs was broken down by Joule self-heating in air at 100 °C. After spin-coating of PMMA, re-burning of the SWNTs at the anode side was triggered by additional voltage application under the WPA condition. (b) Average gap size (or removed length) as a function of applied voltage for SWNT gap extension under WPA, DPA and wet oxygen without PMMA conditions. The channel length was ca. 5 μm. (c) Schematic illustrations for one-way burning from breakdown position under the WPA condition. For clarity, the polymer coating is not shown in the illustrations.

indicates that water vapor plays a critical role in sustaining the burning of SWNTs. The limited reproducibility of the removed length in our previous study [26] conducted in air with PMMA coating can be understood as a strong dependence on the ambient humidity. Moreover, the removed length of SWNTs was decreased by heating the substrates during voltage application [29], which suggests that water molecules adsorbed on the SWNT surfaces [30], rather than those in gas phase, are important for the burning of SWNTs.

The long-length removal of m-SWNTs benefits a single FET, as well as multiple FET fabrication, in two points of view. First, if the m-SWNTs are fully eliminated from the channel, total gate-to-channel capacitance and thus the switching delay will be reduced [31]. Second, formation of m-SWNT nanogaps which localize and amplify the electric field in the vicinity should be avoided because it could lead to unintentional tunneling or breakdown of s-SWNT through electrostatic crosstalk [32].

2.2 One-way re-burning from nanogaps

Although the burning length increased significantly with the assistance of additional water vapor and PMMA coating, it still has a wide distribution from sub-micron to full-length (ca. 10 μm). To understand the origin of the wide distribution, focus was directed on the length of the remaining m-SWNTs on both the cathode (left) and anode (right) sides. Figures 1(d) and (h) show the length of remaining SWNTs after DPA breakdown and WPA burning, respectively. Interestingly, the remaining SWNTs on the cathode side (top panel) had similar length distributions under both conditions, while the anode side (bottom panel) shows completely different features. The remaining SWNT length on the anode side for DPA breakdown was as widely distributed as that on the cathode side. In contrast, most of the remaining SWNTs on the anode side after WPA burning were shorter than 100 nm, and the majority of the SWNTs on the anode side (>80%) were completely removed. Therefore, SWNTs were likely to burn only on the anode side (one-way burning) from the breakdown position, where oxidation of the SWNTs first occurred. This indicates that the burning length was determined almost by the randomly distributed breakdown position.

Re-burning of the SWNTs from the nanogaps formed by electrical breakdown was performed to confirm whether one-way burning could occur during voltage application treatment under the WPA condition. Although SWNTs after electrical breakdown are generally considered to be insulating due to the formation of nanogaps, we have previously shown that nanogaps of SWNTs are extended by an externally applied voltage in the presence of water

vapor due to charge transfer via field emission and water-mediated electrochemical oxidation [29]. Similar observations of nanogaps were conducted after electrical breakdown under various conditions, including the WPA condition.

Electrical breakdown of uncoated SWNTs was conducted in air while the substrate was heated at 100 °C to produce small gaps (ca. 100 nm). Three different ramp voltages (up to 40, 60, and 100 V) were sequentially applied to the broken SWNTs with gaps under the WPA and DPA conditions, and in wet oxygen without the PMMA coating. The top panel of Fig. 2(a) shows an SEM image of two parallel SWNTs, one of which was electrically broken down in air (middle panel). After spin-coating of PMMA and further voltage application under the WPA condition, only the anode side of the lower SWNT was completely removed, while the upper s-SWNT was not burned or damaged (bottom panel). Figure 2(b) shows the average size of extended gaps as a function of the applied voltage for the three conditions examined. The gaps treated under the DPA condition and under wet oxygen without the PMMA coating were enlarged as the applied voltage was increased, similar to our previous study [29]. In contrast, all of the SWNTs at the anode side from the initial gaps were completely removed after the first voltage application (40 V) under the WPA condition, and thus no voltage dependence was observed.

Full-length removal of SWNTs at the anode side under the WPA condition can be attributed to self-sustained burning triggered by voltage-driven etching [29], as schematically presented by steps 2 and 3 in Fig. 2(c). Broken SWNTs with nanogaps, which do not generate Joule heating, will be surrounded by water molecules. Due to the strong field localized within the nanogaps, the SWNT edges at the anode side begin to be etched (step 2). Under the WPA condition, this continuously leads to self-sustained burning of the SWNTs at the anode side, which can propagate along the tube axis without application of an external voltage (step 3). It should be restated that the full-length removal shown in Fig. 2(a) was not caused only by voltage-driven etching [29], in which the gap size changes according to the applied voltage. Small gaps (ca. 100 nm) were always fully extended, as shown in Fig. S6 in the Electronic Supplementary Material (ESM). On the other hand, a relatively large gap (ca. 1 μm) was not extended at all after voltage application up to 100 V, probably because the gap was too large for voltage-driven anode etching to trigger burning of the SWNT. This result excluded voltage-driven etching as the mechanism for the full length removal of SWNTs at the anode side. Therefore, WPA burning can be applied to high-density SWNT arrays without damage to adjacent s-SWNTs via voltage-driven etching.

2.3 Performance of multiple FETs fabricated from purified SWNT arrays

Before further discussing the roles of water and polymer in WPA burning in detail, the effectiveness of the WPA burning was evaluated by the fabrication of multiple FETs after the purification process. The original FETs are defined according to the first electrodes used, i.e., those with SWNTs before and after burning are denoted as FETs A (Fig. 1(a) and (e)) and A′ (Fig. 1(b) and (f)), respectively. After WPA burning or DPA breakdown of the m-SWNTs, second electrodes were added between the original source and drain (first anode and cathode), as schematically illustrated in Fig. 3(a). The two newly defined FETs on the cathode and anode sides are denoted as FETs B and C, respectively. Figure 3(b) shows an SEM image of FETs B (left) and C (right) fabricated from the SWNT array shown in Fig. 1(f).

The on/off ratios of the A, A′, B and C FETs for both WPA burning and DPA breakdown are plotted in Fig. 3(c). The A FETs showed on/off ratios below 10, which indicates the coexistence of both m- and s- SWNTs in the original channels (typically composed of ca. 30 SWNTs). The A′ FETs after both WPA burning and DPA breakdown showed on/off ratios in the range of 10^3–10^6, which indicates that all the m-SWNTs were broken down. Importantly, the C FETs at the anode side after WPA burning had on/off ratios almost as high as the A′ FETs because the m-SWNTs that remained at the anode side were very short. In contrast, the B FETs at the cathode side showed low on/off ratios due to the short circuit caused by the m-

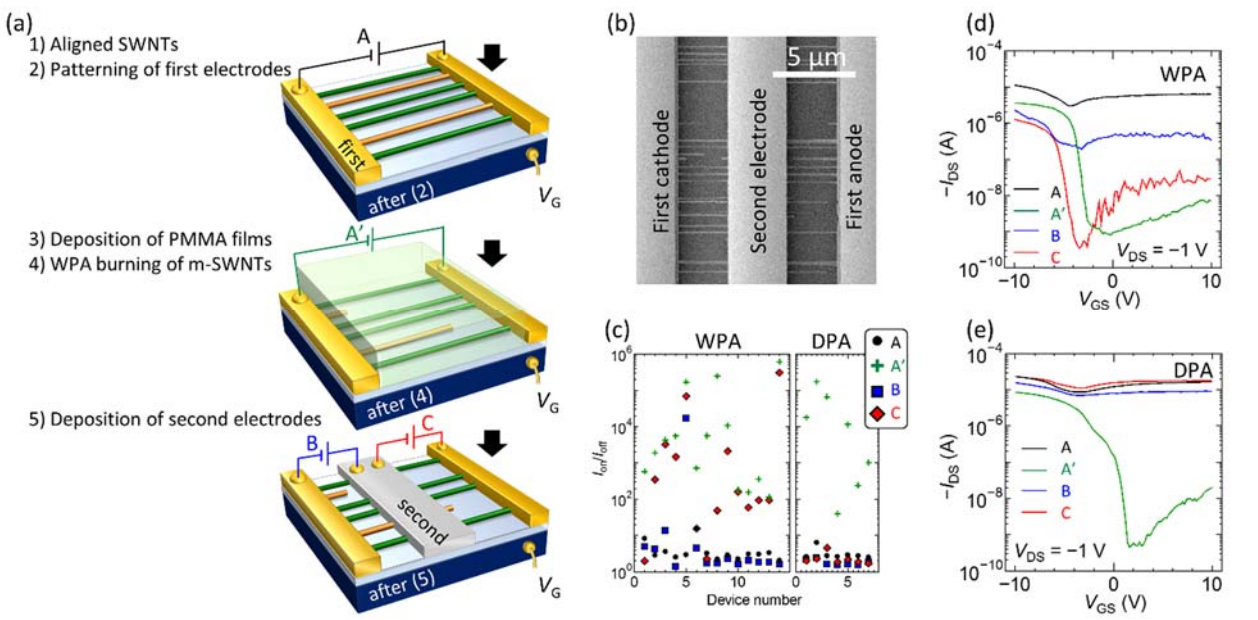

Figure 3 (a) Schematic illustration of the fabrication of multiple FETs after WPA burning. Two FETs were newly defined by the addition of an extra gold electrode between the original source and drain electrodes, after WPA burning of the m-SWNTs. (b) SEM image of redefined FETs. Left (cathode side) and right (anode side) FETs are denoted as B and C, respectively. (c) On/off ratios of FETs A, A', B, and C for WPA burning (left). Similar data for DPA breakdown are plotted on the right for comparison. (d,e) Typical transfer characteristics for the four types of FETs subjected to (d) WPA burning and (e) DPA breakdown. V_{DS} = -1 V.

SWNTs that remained at the cathode side. This result is consistent with the SEM observation shown in Fig. 1. The device performance confirmed that the long length of the m-SWNTs was removed by WPA burning. Raman spectroscopy, optical microscopy with crossed polarizers [33], and atomic force microscopy (AFM) measurements supported the selective and long-length removal of m-SWNTs by WPA burning (Fig. S7–9 in the ESM). However, for DPA breakdown, whereby the remaining SWNT length at both the cathode and anode sides was long, both the B and C FETs had on/off ratios of less than 10.

Figures 3(d) and (e) show transfer characteristics for the A (black), A' (green), B (blue), and C (red) FETs after the WPA burning and DPA breakdown processes, respectively. The on current was decreased by 75±19% after WPA burning, while that after DPA breakdown was 79±23%, which indicates that additional water vapor did not deteriorate the selectivity toward the electrical breakdown of m-SWNTs. It should be stressed that the reduction of on current after WPA burning is comparable to that after thermocapillary flow and reactive ion etching [19], in which all s-SWNTs were considered to be preserved with the assumption of a typical ratio of population and conductance of s- and m-SWNTs. Under the similar assumption, the number-based purity of s-SWNTs is calculated to be 99.8% for WPA burning based on the device performance.

The fabrication of multiple FETs thus demonstrates the potential of WPA burning as a large-scale purification process, although the burning length should be further improved. The remaining SWNT length at the cathode side was highly dependent on the location of initial gap formation; therefore, the breakdown position should be controlled to obtain a high on/off ratio for a larger number of FETs. In this sense, re-burning from nanogaps should be exploited because it can be separated from the gap formation process at controlled positions and it would broaden the chance to achieve full-length removal of m-SWNTs.

2.4 Discussion on the roles of water and polymer in the burning process

A possible role of water molecules in the burning process is substantial enhancement of the oxidation rate of both SWNTs and PMMA films due to adsorption on the SWNTs. The addition of water vapor to the feed gas (typically oxygen) is known to increase the oxidation rate of graphite [34]. Water itself can also be used in hydrogen production through coal gasification [35]. The interval of oxygen collision with a carbon atom of an SWNT under the experimental conditions employed (ca. 90 kPa oxygen) is typically ca. 10^{-9} s. This is much larger than the thermal relaxation time [36] (ca. 10^{-10} s) of an SWNT on a SiO_2 substrate. Furthermore, the reaction rate is much smaller than the collision rate due to the activation energy. The oxidation induced by gas molecule collision is thus unlikely to result in a chain reaction of SWNT burning. We propose that the adsorbed water acts as an oxidizer and significantly increases the oxidation rate of both SWNTs and PMMA because water molecules can be adsorbed on SWNT surfaces and readily involved in the reaction with SWNTs. The oxidation of SWNTs by water ($C(s) + H_2O(l) \rightarrow CO(g) + H_2(g)$) is an endothermic reaction; therefore, this reaction cannot be self-propagated. Chemical reaction products, such as CO and H_2, can generate heat by reaction with oxygen in the vicinity of the SWNTs. Water may thus contribute to the burning of SWNTs catalytically through multiple complicated reactions.

Figure 2c schematically shows how Joule self-heating leads to one-way burning from randomly scattered breakdown positions under the WPA condition. Nanogap formation (step 1) and voltage-triggered re-burning (step 3) must occur sequentially; otherwise, all the SWNTs would burn in both directions from the breakdown position. The adsorption and desorption of water vapor onto/from SWNTs are likely to be involved in this sequential phenomenon. The similarity of the breakdown power density and breakdown voltage for burning under the DPA and WPA conditions (Fig. S4 in the ESM) suggests that water vapor does not influence the initial gap formation process, because water molecules are desorbed from hot SWNTs during Joule heating. The dependence of breakdown power on the oxygen partial pressure (Fig. S1 in the ESM) also indicates that SWNT breakdown is provoked only by oxygen gas.

When the SWNTs are broken down and nanogaps are formed, water molecules can be adsorbed or even encapsulated [37] on/in the SWNTs, which quickly cooled down to room temperature. The bias voltage is continuously applied after nanogap formation; therefore, the amplified field at the nanogaps induces re-burning of the SWNTs at the anode side. Although the temperature of the burning SWNT edge is very high, the hot region is localized near the reaction front, as later suggested in Section 2.5. In addition, the velocity of SWNT burning should be greater than ca. 1000 m s^{-1} for the chain-reaction to be self-sustained, according to the simulation (see Section 2.5). It is quite possible that the adsorbed water molecules are involved in the reaction with SWNTs before desorption from the SWNTs during WPA burning.

The removed length of SWNTs was also measured in wet oxygen gas without PMMA coating (Fig. S3 in the ESM) to evaluate the importance of the PMMA film. The length of removed portion of SWNTs was increased to 1.32 μm on average by the addition of water vapor, but this was much smaller than that with the WPA condition. When polymer-assisted burning was performed in air with a relative humidity of <20%, the use of PMMA films slightly increased the average length removed from 0.30 to 0.82 μm (Fig. S3 in the ESM). Therefore, the combination of PMMA coating and high-pressure water vapor is essential for the full-length removal of m-SWNTs. PMMA has another role to avoid lateral etching, which is caused by the interconnection of SWNTs via the occasional formation of water droplets on the substrates under high humidity. Therefore, PMMA coating facilitates the high selectivity of electrical breakdown between s- and m-SWNTs in the presence of saturated water vapor.

PMMA thin films (ca. 26 nm thick) do not suppress the supply of oxygen to SWNTs. The power needed to break SWNTs was strongly dependent on the collision frequency of oxygen, which is proportional to the oxygen partial pressure (Fig. S1 in the ESM). On the other hand, the coating of SWNTs with PMMA did not

significantly change the breakdown power (Fig. S2 in the ESM), while thicker PMMA films (ca. 500 nm) increased the breakdown power by >10%. This indicates that the thinner coating has less influence on gas diffusion in the vicinity of the SWNTs, and is likely to be beneficial to the self-sustainable burning of SWNTs. PMMA coating on SWNTs was previously used as a passivation layer to reduce hysteresis in the transfer characteristics of FETs by the removal of water from the vicinity of the SWNTs [38]. In contrast, the PMMA-coated FETs in the present experiments were p-doped by exposure to the wet oxygen and exhibited a reduction of ambipolar features compared to that measured in a vacuum. Therefore, oxygen and water molecules are likely to easily penetrate through the PMMA thin films employed in this study.

2.5 Simulation of polymer-coated SWNT burning

Simulations of m-SWNT burning were performed with a device configuration to represent the SWNT samples and to further discuss the role of the polymer coating in the enhancement of SWNT burning. The theory of conventional combustion waves was adopted in a similar way to that in the literature [39]. For simplicity, only one-dimensional distribution of temperature and oxidation reaction was considered for both an SWNT and a 2-nm-thick polymer layer in the vicinity of the SWNT (hereafter referred to as the inner PMMA). Figures 4(a-c) show the SiO_2 substrate and the PMMA film other than the inner PMMA (denoted as outer PMMA) are kept at room temperature (T_0) because the substrate temperature will not be increased significantly due to large thermal boundary resistance with SWNTs. This system is described by the following equations:

$$\rho_1 c_1 A_1 \frac{\partial}{\partial t} T_1(x,t) = \kappa_1 A_1 \frac{\partial^2 T_1}{\partial x^2} + \frac{\rho_1 A_1 Q_1}{M_{W1}} \frac{\partial \eta_1}{\partial t} - g_{sub}(T_1 - T_0) - g_{poly}(T_1 - T_2), \quad (1)$$

$$\frac{\partial}{\partial t} \eta_1(x,t) = k_1 (1 - \eta_1) \exp\left(-\frac{E_{a1}}{R T_1}\right), \quad (2)$$

$$\rho_2 c_2 A_2 \frac{\partial}{\partial t} T_2(x,t) = \kappa_2 A_2 \frac{\partial^2 T_2}{\partial x^2} + \frac{\rho_2 A_2 Q_2}{M_{W2}} \frac{\partial \eta_2}{\partial t} - g_{out}(T_2 - T_0) - g_{poly}(T_2 - T_1), \quad (3)$$

$$\frac{\partial}{\partial t} \eta_2(x,t) = k_2 (1 - \eta_2) \exp\left(-\frac{E_{a2}}{R T_2}\right), \quad (4)$$

where subscripts 1 and 2 indicate an SWNT and a PMMA layer, respectively, ρ is the mass density, c is the specific heat capacity, T is the temperature as a function of axial position x and time t, κ is the thermal conductivity, A is the cross-section, Q is the heat of combustion, M_w is the molecular weight, g_{sub} is the thermal boundary conductance (TBC) at the SWNT/SiO_2 interface per length, g_{poly} is the TBC at the SWNT/PMMA interface, and g_{out} is the TBC at an imaginary interface of the inner/outer PMMA. η is the extent of oxidation ($0 \le \eta \le 1$), E_a is the activation energy of the oxidation reaction, k is the Arrhenius prefactor (collision rate), and R is the gas constant. Parameters used in the simulation are listed in Table 1 [40–43]. g_{sub} and E_{a1} were estimated from preliminary experiments (Fig. S1 and S2 in the ESM). g_{out} is presumed to be 30 MW m^{-1} K^{-1}, based on a two-dimensional temperature simulation (Fig. S10 in the

Table 1 Parameters used in the simulation of SWNT-PMMA burning. All the simulation results were obtained using these parameters, unless otherwise mentioned.

Chirality (n,m)	L_{ch} [μm]	κ_1 (@ 300 K) [W m^{-1} K^{-1}]	κ_2 [W m^{-1} K^{-1}]	$k_{1,2}$ [s^{-1}]	g_{sub}/d_t [W m^{-1} K^{-1}]	g_{poly}/A_{wall} [W m^{-1} K^{-1}]	E_{a1} [eV]	E_{a2} [eV]
10,10	3	1×10^{3}†	0.2	1×10^{14}	2.0×10^{7}‡	1.3×10^{7}	1.4	0.6§

† The same temperature dependence [40] as that in the literature was given for the thermal conductivity κ_1. An intermediate value between theoretical [43] and experimental [40] studies was employed as the absolute value of κ_1 in this study.

‡ The TBC at the SWNT/polyethylene interface based on molecular dynamics [41] was used instead of that at the SWNT/PMMA interface.

§ Among the various levels of PMMA oxidation, the lowest activation energy based on thermogravimetry [42] was used here.

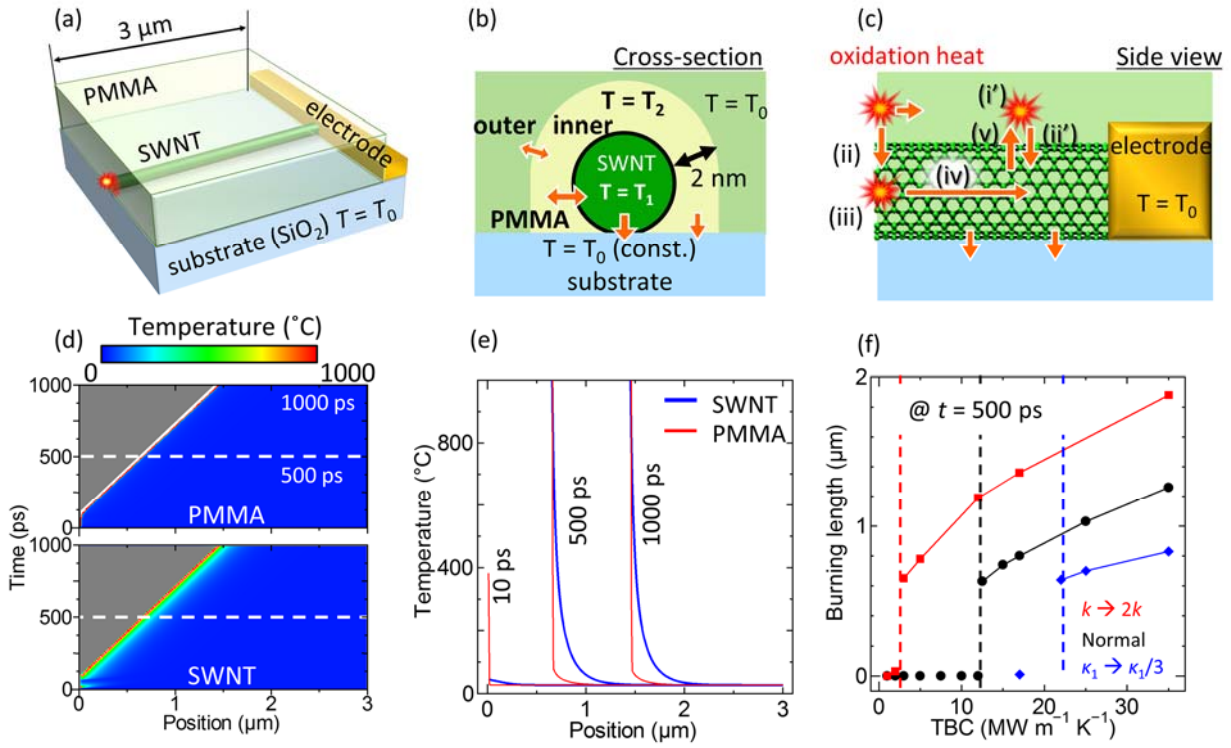

Figure 4 (a) Schematic illustration of the simulation setup. One side of a 3-μm-long SWNT on a SiO_2 substrate (= T_0) is connected to metal electrodes (= T_0). (b) Cross-sectional and (c) side views of the heat flow model. For simplicity, the 2-nm-thick PMMA layer has variable temperature and is surrounded by the outer PMMA film, which is kept at room temperature (= T_0). (d) Simulated time-profile of temperature distribution along a PMMA-coated SWNT. The burned regions of the SWNT and PMMA are shown in gray. (e) 1D temperature profiles of the SWNT (blue) and the inner PMMA (red) at various times. (f) Dependence of the simulated burning length at t = 500 ps on TBC at the SWNT/PMMA interface. Results for high Arrhenius prefactor $k_{1,2}$ and low SWNT thermal conductivity κ_1 are also shown in red and blue, respectively.

ESM). An appropriate value of the Arrhenius prefactor k for the oxidation of SWNTs and PMMA, especially when water molecules are involved in the oxidation reaction, has not yet been reported. Therefore, after determining the other parameters, the Arrhenius prefactor we adjusted to be 1×10^{14} s^{-1}, so that oxidation of PMMA-coated SWNTs was self-propagated. This extremely large value roughly corresponds to the frequency of molecular vibration and can be interpreted as the direct supply of water molecules as an oxidant from the adsorbed layers.

The temperature of the edge (20 nm in length) of an SWNT and the surrounding PMMA was set at 573 K to simulate the burning initiated by voltage-driven etching (Fig. 2). The burning of the SWNTs coated with PMMA was self-propagated along the axis, as shown by the temperature-time profiles of the SWNT (bottom) and inner PMMA (top) in Fig. 4(d). Figure 4(e) shows the one-dimensional temperature distribution of the SWNT and inner PMMA at three different times (t = 10, 500, and 1000 ps) after ignition. The thermal conductivity of SWNTs is much higher than that of PMMA, so that the SWNT conducted more heat and had a gentler temperature gradient than PMMA.

Figure 4(f) shows the burning length at t = 500 ps as a function of the TBC at the SWNT/PMMA interface with various Arrhenius prefactor k, or thermal conductivity of SWNTs, κ_1. When the TBC g_{poly} was lower than the threshold, burning did not propagate. Efficient heat flow between SWNTs and PMMA films is thus required for the self-sustained burning of SWNTs. On the other hand, SWNT burning without

the PMMA coating can be simulated by setting the TBC at the SWNT/PMMA interface to zero, which results in no propagation of burning, even when the temperature of the edge is set much higher than 573 K. Simulation for low thermal conductivity of SWNTs, as shown in Fig. 4(f) (blue), indicates that thermal conductivity is also an important factor to achieve self-propagation of SWNT-PMMA burning. SWNTs are one-dimensional materials that have high thermal conductivity only in the axial direction; therefore, lateral propagation of the burning via the PMMA thin films, which could result in the removal of s-SWNTs, is unlikely to occur. It should be stressed that when the Arrhenius prefactor is set at 1×10^{9} s^{-1}, which is similar to the collision frequency of oxygen to carbon atoms of SWNTs in ambient air, the oxidation reaction was very quickly terminated.

The burning of SWNTs and PMMA can be summarized as follows. The inner PMMA begins to oxidize (step i in Fig. 4(c)) in advance of the SWNT due to its lower activation energy, and then heats the SWNT from the outside (step ii), which induces SWNT oxidation (step iii). The large amount of heat at the reaction front is then effectively transferred along the SWNT axis (step iv). The transferred heat then induces subsequent oxidation of the adjacent PMMA (step v). This cycle (steps i–v) occurs repeatedly, and results in self-propagation of SWNT and PMMA burning.

We have previously considered that uniform Joule self-heating along SWNTs is necessary to achieve full-length burning, assuming that oxidation should propagate before the electrically heated SWNTs are cooled down [26]. However, this assumption is contradicted by the simulation without Joule self-heating (Fig. 4(d)). The importance of uniform Joule self-heating is also excluded by the experimental results for re-burning from nanogaps (Fig. 2). The burning of SWNTs is self-sustained, despite the fast cooling; therefore, it would propagate over any length until contact with the metal electrodes, unless non-uniformities are present (Fig. S12 in the ESM). Ideally, an arbitrary length of SWNTs can be therefore removed by WPA burning, as demonstrated by the full-length experimental burning of 29-μm-long SWNTs (Fig. S5 in the ESM).

3 Conclusions

The water- and polymer-assisted burning of m-SWNTs towards the formation of s-SWNT arrays was presented. The addition of water vapor to the system significantly enhanced the oxidation rate of SWNTs, which led to self-sustained burning of the SWNTs. The fabrication of multiple FETs after burning demonstrated the advantage of long-length removal of m-SWNTs as a large-scale purification process over conventional electrical breakdown. One-way burning from a random location of gap formation to the anode resulted in the residual m-SWNT segments near the one side. Therefore, control of the breakdown position is necessary for the complete full-length removal of m-SWNTs and the formation of high-density purely semiconducting SWNT arrays for application in large-scale electronics.

4 Methods

4.1 SWNT growth. R-cut quartz was used for aligned growth. Quartz substrates were initially annealed at 900 °C in air. An Fe catalyst (0.2 nm thick) was photolithographically patterned into parallel stripes using thermal evaporation, followed by lift-off and heating at 500 °C in air. SWNTs were grown at 800 °C with ethanol as a feedstock gas [44,45].

4.2 Electrode Patterning. Initial electrodes (Ti/Pt, typically 2/23 nm) were photolithographically patterned on as-delivered silicon substrates (SUMCO Corp., highly p-doped Si with 100-nm-thick oxide layer) by sputtering. Bilayer resist (polydimethylglutarimide as a sacrificial layer) and thin metal layers were exploited to obtain electrodes with smooth edges. Here, p-doped silicon substrates functioned as a global back gate.

4.3 SWNT transfer. 4 wt% PMMA [46] solution in anisole was spin-coated at 2000 rpm onto quartz substrates on which the SWNTs were grown, and the

substrates were then heated at 170 °C in air for 15 min. After scratching the substrate surface near the edges with a diamond knife, the substrates were immersed in aqueous KOH (1 mol L^{-1}) and heated to 100 °C for 10 min. The PMMA thin film was spontaneously peeled off from the substrate when placed in cold distilled water, and then picked up by the target substrates with pre-patterned electrodes after rinsing. After natural drying in air at room temperature, the substrate was heated to 170 °C for 30 min. Finally, the PMMA films were dissolved in acetone, followed by annealing in vacuum at 350 °C for 3 h. The alignment of the SWNT arrays should be maintained during the transfer process because bundled SWNTs are burned together, regardless of the metallicity of the SWNTs, if the bundle contains at least one m-SWNTs. After transfer of the SWNT arrays, unwanted SWNTs were etched away using oxygen plasma, while SWNTs in the channel region were protected by the photoresist.

4.4 SWNT burning initiated by Joule self-heating. SWNTs were typically burned by ramping the drain voltage from 0 V to a negative value until drain current became sufficiently small (typically up to V_{DS} = –6 V μm^{-1}), while a positive gate voltage (V_{GS} = 10 V) was applied to turn the s-SWNTs off. 1 wt% PMMA ($M_W \approx 996{,}000$) solution in anisole was spin-coated at 3000 rpm onto the substrates with SWNT arrays, followed by heating at 170 °C in air for 15 min. The thickness of the PMMA film was ca. 26 nm (measured using AFM). The ambient gas during SWNT burning was controlled as follows. A vacuum probe station connected to an oxygen gas cylinder and a water tank was used to control the ambient gas. After evacuation of the chamber to vacuum with a rotary pump, oxygen and water vapor were introduced into the chamber. Oxygen gas (90 kPa total pressure) with relative humidities of 0% or 100% was typically used. Although a bottom-contact structure by transfer of the SWNTs onto electrodes was employed in this study, the same burning behavior of SWNTs was obtained for a top-contact geometry.

Acknowledgements

Part of this work was financially supported by JSPS KAKENHI Grant Number JP15H05760, JP25107002, JP26420135 and JST-EC DG RTD within the Strategic International Collaborative Research Program (SICORP). This work was partly conducted at the Center for Nano Lithography & Analysis, VLSI Design and Education Center (VDEC), and at the Laser Alliance of the University of Tokyo. K.O. was financially supported by a JSPS Fellowship (JP15J07857).

Electronic Supplementary Material: Supplementary material (further details of breakdown power of SWNTs, comparison of removed length under various conditions, re-burning from SWNT nanogaps, confirmation of SWNT removal by Raman spectroscopy and AFM, and simulation of SWNT burning) is available in the online version of this article at http://dx.doi.org/10.1007/s12274-***-****-* (automatically inserted by the publisher).

References

[1] Shulaker, M. M.; Hills, G.; Patil, N.; Wei, H.; Chen, H.-Y.; Wong, H.-S. P.; Mitra, S. Carbon Nanotube Computer. *Nature* **2013**, *501*, 526–530.

[2] Franklin, A. D. Electronics: The Road to Carbon Nanotube Transistors. *Nature* **2013**, *498*, 443–444.

[3] Kocabas, C.; Hur, S.-H.; Gaur, A.; Meitl, M. a; Shim, M.; Rogers, J. A. Guided Growth of Large-Scale, Horizontally Aligned Arrays of Single-Walled Carbon Nanotubes and Their Use in Thin-Film Transistors. *Small* **2005**, *1*, 1110–1116.

[4] Ago, H.; Nakamura, K.; Ikeda, K.; Uehara, N.; Ishigami, N.; Tsuji, M. Aligned Growth of Isolated Single-Walled Carbon Nanotubes Programmed by Atomic Arrangement of Substrate Surface. *Chem. Phys. Lett.* **2005**, *408*, 433–438.

[5] Hu, Y.; Kang, L.; Zhao, Q.; Zhong, H.; Zhang, S.; Yang, L.; Wang, Z.; Lin, J.; Li, Q.; Zhang, Z.; *et al.* Growth of High-Density Horizontally Aligned SWNT Arrays Using Trojan Catalysts. *Nat. Commun.* **2015**, *6*, 6099.

[6] Kang, L.; Hu, Y.; Zhong, H.; Si, J.; Zhang, S.; Zhao, Q.; Lin, J.; Li, Q.; Zhang, Z.; Peng, L.; *et al.* Large-Area Growth of Ultra-High-Density Single-Walled Carbon Nanotube Arrays on Sapphire Surface. *Nano Res.* **2015**, *8*, 3694.

[7] Zhou, W.; Ding, L.; Yang, S.; Liu, J. Synthesis of High-Density, Large-Diameter, and Aligned Single-Walled Carbon Nanotubes by Multiple-Cycle Growth Methods.

ACS Nano **2011**, *5*, 3849–3857.

[8] Hong, S. W.; Banks, T.; Rogers, J. A. Improved Density in Aligned Arrays of Single-Walled Carbon Nanotubes by Sequential Chemical Vapor Deposition on Quartz. *Adv. Mater.* **2010**, *22*, 1826–1830.

[9] Shulaker, M. M.; Wei, H.; Payne, J.; Provine, J.; Chen, H.; Wong, H.-S. P.; Mitra, S. Linear Increases in Carbon Nanotube Density through Multiple Transfer Technique. *Nano Lett.* **2011**, *11*, 1881–1886.

[10] Engel, M.; Small, J. P.; Steiner, M.; Freitag, M.; Green, A. A.; Hersam, M. C.; Avouris, P. Thin Film Nanotube Transistors Based on Self-Assembled, Aligned, Semiconducting Carbon Nanotube Arrays. *ACS Nano* **2008**, *2*, 2445–2452.

[11] Shekhar, S.; Stokes, P.; Khondaker, S. I. Ultrahigh Density Alignment of Carbon Nanotube Arrays by Dielectrophoresis. *ACS Nano* **2011**, *5*, 1739–1746.

[12] Cao, Q.; Han, S.-J.; Tulevski, G. S. Fringing-Field Dielectrophoretic Assembly of Ultrahigh-Density Semiconducting Nanotube Arrays with a Self-Limited Pitch. *Nat. Commun.* **2014**, *5*, 5071.

[13] Brady, G. J.; Way, A. J.; Safron, N. S.; Evensen, H. T.; Gopalan, P.; Arnold, M. S. Quasi-Ballistic Carbon Nanotube Array Transistors with Current Density Exceeding Si and GaAs. *Sci. Adv.* **2016**, *2*, e1601240–e1601240.

[14] Zhou, W.; Zhan, S.; Ding, L.; Liu, J. General Rules for Selective Growth of Enriched Semiconducting Single Walled Carbon Nanotubes with Water Vapor as in Situ Etchant. *J. Am. Chem. Soc.* **2012**, *134*, 14019–14026.

[15] Yang, F.; Wang, X.; Zhang, D.; Yang, J.; Xu, Z.; Wei, J.; Wang, J.-Q.; Xu, Z.; Peng, F.; Li, X.; *et al.* Chirality-Specific Growth of Single-Walled Carbon Nanotubes on Solid Alloy Catalysts. *Nature* **2014**, *510*, 522–524.

[16] Kang, L.; Zhang, S.; Li, Q.; Zhang, J. Growth of Horizontal Semiconducting SWNT Arrays with Density Higher than 100 Tubes/μm Using Ethanol/Methane Chemical Vapor Deposition. *J. Am. Chem. Soc.* **2016**, *138*, 6727–6730.

[17] Collins, P. G.; Arnold, M. S.; Avouris, P. Engineering Carbon Nanotubes and Nanotube Circuits Using Electrical Breakdown. *Science* **2001**, *292*, 706–709.

[18] Zhang, G.; Qi, P.; Wang, X.; Lu, Y.; Li, X.; Tu, R.; Bangsaruntip, S.; Mann, D. A.; Zhang, L.; Dai, H. Selective Etching of Metallic Carbon Nanotubes by Gas-Phase Reaction. *Science* **2006**, *314*, 974–977.

[19] Jin, S. H.; Dunham, S. N.; Song, J.; Xie, X.; Kim, J.-H.; Lu, C.; Islam, A. E.; Du, F.; Kim, J.; Felts, J.; *et al.* Using Nanoscale Thermocapillary Flows to Create Arrays of Purely Semiconducting Single-Walled Carbon Nanotubes. *Nat. Nanotechnol.* **2013**, *8*, 347–355.

[20] Li, J.; Franklin, A. D.; Liu, J. Gate-Free Electrical Breakdown of Metallic Pathways in Single-Walled Carbon Nanotube Crossbar Networks. *Nano Lett.* **2015**, *15*, 6058–6065.

[21] Shulaker, M. M.; Pitner, G.; Hills, G.; Giachino, M.; Wong, H.-S. P.; Mitra, S. High-Performance Carbon Nanotube Field-Effect Transistors. In *2014 IEEE International Electron Devices Meeting*; 2014; Vol. 4, p. 33.6.1-33.6.4.

[22] Shulaker, M. M.; Van Rethy, J.; Hills, G.; Wei, H.; Chen, H.-Y.; Gielen, G.; Wong, H.-S. P.; Mitra, S. Sensor-to-Digital Interface Built Entirely With Carbon Nanotube FETs. *IEEE J. Solid-State Circuits* **2014**, *49*, 190–201.

[23] Patil, N.; Lin, A.; Zhang, J.; Wei, H.; Anderson, K.; Philip Wong, H.-S.; Mitra, S. Scalable Carbon Nanotube Computational and Storage Circuits Immune to Metallic and Mispositioned Carbon Nanotubes. *IEEE Trans. Nanotechnol.* **2011**, *10*, 744–750.

[24] Shulaker, M. M.; Van Rethy, J.; Wu, T. F.; Suriyasena Liyanage, L.; Wei, H.; Li, Z.; Pop, E.; Gielen, G.; Wong, H.-S. P.; Mitra, S. Carbon Nanotube Circuit Integration up to Sub-20 Nm Channel Lengths. *ACS Nano* **2014**, *8*, 3434–3443.

[25] Pop, E. The Role of Electrical and Thermal Contact Resistance for Joule Breakdown of Single-Wall Carbon Nanotubes. *Nanotechnology* **2008**, *19*, 295202.

[26] Otsuka, K.; Inoue, T.; Chiashi, S.; Maruyama, S. Selective Removal of Metallic Single-Walled Carbon Nanotubes in Full Length by Organic Film-Assisted Electrical Breakdown. *Nanoscale* **2014**, *6*, 8831–8835.

[27] Liao, A. D.; Alizadegan, R.; Ong, Z.-Y.; Dutta, S.; Xiong, F.; Hsia, K. J.; Pop, E. Thermal Dissipation and Variability in Electrical Breakdown of Carbon Nanotube Devices. *Phys. Rev. B* **2010**, *82*, 205406.

[28] Xie, X.; Grosse, K. L.; Song, J.; Lu, C.; Dunham, S. N.; Du, F.; Islam, A. E.; Li, Y.; Zhang, Y.; Pop, E.; *et al.* Quantitative Thermal Imaging of Single-Walled Carbon Nanotube Devices by Scanning Joule Expansion Microscopy. *ACS Nano* **2012**, *6*, 10267–10275.

[29] Otsuka, K.; Inoue, T.; Shimomura, Y.; Chiashi, S.; Maruyama, S. Field Emission and Anode Etching during Formation of Length-Controlled Nanogaps in Electrical Breakdown of Horizontally Aligned Single-Walled Carbon Nanotubes. *Nanoscale* **2016**, *8*, 16363–16370.

[30] Homma, Y.; Chiashi, S.; Yamamoto, T.; Kono, K.; Matsumoto, D.; Shitaba, J.; Sato, S. Photoluminescence Measurements and Molecular Dynamics Simulations of Water Adsorption on the Hydrophobic Surface of a Carbon Nanotube in Water Vapor. *Phys. Rev. Lett.* **2013**, *110*, 157402.

[31] Cao, Q.; Xia, M.; Kocabas, C.; Shim, M.; Rogers, J. a.; Rotkin, S. V. Gate Capacitance Coupling of Singled-Walled Carbon Nanotube Thin-Film Transistors. *Appl. Phys. Lett.* **2007**, *90*, 23516.

[32] Wahab, M. A.; Alam, M. A. Implications of Electrical Crosstalk for High Density Aligned Array of Single-Wall Carbon Nanotubes. *IEEE Trans. Electron Devices* **2014**,

61, 4273–4281.

[33] Deng, S.; Tang, J.; Kang, L.; Hu, Y.; Yao, F.; Zhao, Q.; Zhang, S.; Liu, K.; Zhang, J. High-Throughput Determination of Statistical Structure Information for Horizontal Carbon Nanotube Arrays by Optical Imaging. *Adv. Mater.* **2016**, *28*, 2018–2023.

[34] Matsui, K.; Tsuji, H.; Makino, A. A Further Study of the Effects of Water Vapor Concentration on the Rate of Combustion of an Artificial Graphite in Humid Air Flow. *Combust. Flame* **1986**, *63*, 415–427.

[35] Jensen, G. A. The Kinetics of Gasification of Carbon Contained in Coal Minerals at Atmospheric Pressure. *Ind. Eng. Chem. Process Des. Dev.* **1975**, *14*, 308–314.

[36] Ong, Z.-Y.; Pop, E. Molecular Dynamics Simulation of Thermal Boundary Conductance between Carbon Nanotubes and SiO2. *Phys. Rev. B* **2010**, *81*, 155408.

[37] Chiashi, S.; Hanashima, T.; Mitobe, R.; Nagatsu, K.; Yamamoto, T.; Homma, Y. Water Encapsulation Control in Individual Single-Walled Carbon Nanotubes by Laser Irradiation. *J. Phys. Chem. Lett.* **2014**, *5*, 408–412.

[38] Kim, W.; Javey, A.; Vermesh, O.; Wang, Q.; Li, Y.; Dai, H. Hysteresis Caused by Water Molecules in Carbon Nanotube Field-Effect Transistors. *Nano Lett.* **2003**, *3*, 193–198.

[39] Choi, W.; Hong, S.; Abrahamson, J. T.; Han, J.-H.; Song, C.; Nair, N.; Baik, S.; Strano, M. S. Chemically Driven Carbon-Nanotube-Guided Thermopower Waves. *Nat. Mater.* **2010**, *9*, 423–429.

[40] Pop, E.; Mann, D. A.; Wang, Q.; Goodson, K. E.; Dai, H. Thermal Conductance of an Individual Single-Wall Carbon Nanotube above Room Temperature. *Nano Lett.* **2006**, *6*, 96–100.

[41] Hida, S.; Hori, T.; Shiga, T.; Elliott, J.; Shiomi, J. Thermal Resistance and Phonon Scattering at the Interface between Carbon Nanotube and Amorphous Polyethylene. *Int. J. Heat Mass Transf.* **2013**, *67*, 1024–1029.

[42] Hirata, T.; Kashiwagi, T.; Brown, J. E. Thermal and Oxidative Degradation of Poly(methyl Methacrylate): Weight Loss. *Macromolecules* **1985**, *18*, 1410–1418.

[43] Maruyama, S. A Molecular Dynamics Simulation of Heat Conduction in Finite Length SWNTs. *Phys. B Condens. Matter* **2002**, *323*, 193–195.

[44] Maruyama, S.; Kojima, R.; Miyauchi, Y.; Chiashi, S.; Kohno, M. Low-Temperature Synthesis of High-Purity Single-Walled Carbon Nanotubes from Alcohol. *Chem. Phys. Lett.* **2002**, *360*, 229–234.

[45] Inoue, T.; Hasegawa, D.; Badar, S.; Aikawa, S.; Chiashi, S.; Maruyama, S. Effect of Gas Pressure on the Density of Horizontally Aligned Single-Walled Carbon Nanotubes Grown on Quartz Substrates. *J. Phys. Chem. C* **2013**, *117*, 11804–11810.

[46] Jiao, L.; Fan, B.; Xian, X.; Wu, Z.; Zhang, J.; Liu, Z. Creation of Nanostructures with Poly(methyl Methacrylate)-Mediated Nanotransfer Printing. *J. Am. Chem. Soc.* **2008**, *130*, 12612–12613.